

Width of Phonon Sidebands in the Brownian Oscillator Model

Jun Ye and Yang Zhao*

School of Materials Science and Engineering, Nanyang Technology University, Singapore 639798

Nathaniel Ng

Materials Theory and Simulation Laboratory, Institute of High Performance Computing, Singapore 138632

Jianshu Cao

Department of Chemistry, Massachusetts Institute of Technology, Cambridge, Massachusetts 02139

Received: October 24, 2008; Revised Manuscript Received: January 19, 2009

The line width dependence of zero-phonon lines and phonon sidebands on temperature, bath dissipation, and electron–phonon coupling is studied for an underdamped Brownian oscillator model with an Ohmic dissipative bath. Factors determining the line widths vary from the zero-phonon lines to the phonon sidebands. The control-parameter space of line broadening has been mapped out, revealing that the line widths of the zero-phonon lines and phonon sidebands are linearly dependent on both the temperature and the Huang–Rhys factor. It is also found that the dependence of the line widths on the bath damping factor is linear for the zero-phonon lines and quadratic for the phonon sidebands.

I. Introduction

A nanocrystal (NC) is typically made of hundreds or thousands of atoms. With a size of 1–10 nm, it is considered as a quantum dot (QD). Since NCs are larger than individual atoms, yet much smaller than materials in bulk, their unique electronic, optical, and mechanical properties are of great fundamental and applicational interest. In bulk CdSe, for example, the Bohr radius of an exciton is around 5.6 nm (emitting only red light), but in an NC, CdSe can have a much smaller Bohr radius. Engineering the optical properties of the NCs by controlling their growth (size, shape, materials, coatings, etc.) makes NCs quite appealing for many optical applications such as spectra engineering for light emissions across the entire visible spectrum. Theory on optical properties of NCs, however, lags far behind their fabrication technologies. Many fundamental questions remain largely unanswered: What is the temperature dependence of the exciton absorption energy? What causes the Stokes shift and its temperature dependence? What is the homogeneous line width of a single NC? Developing a physical model to explain these NC properties is essential for NC design.

Efros calculated energy spectra of holes in CdSe NCs with hexagonal lattices,¹ and Bawendi and co-workers found a fine structure with five levels which are formed from an 8-fold degenerate bulk band edge exciton.² Exciton thermalization to the lowest QD state, which is optically forbidden, explains the long-lived nature of the optical emission. Takagahara derived expressions for electron–phonon interactions in semiconductor NCs, and studied the size dependence of the coupling strength for representative coupling mechanisms.³ For Si NCs the Huang–Rhys factor and the Stokes shift of photoluminescence due to acoustic phonons were calculated and their size dependence is clarified. A dephasing term that is linearly dependent on temperature and inversely proportional to the square of the NC size is attributed to the deformation potential. Other recent

contributions concerning the effects of electron–phonon coupling on NC optical properties include refs 4–7. It is worth mentioning that a nonperturbative approach is employed to calculate the polaronic effects in QDs taking into account electronic levels coupled via interactions with several confined phonon modes.⁴

Schmitt-Rink and co-workers made a few early predictions on the effect of the diminishing size of the QDs on their optical properties.⁸ For example, they pointed out a useful range of QD sizes for which the electronic states are similar to those of crystalline semiconductors and can be described by the effective mass approximation (using envelope functions for confinement effects). The coupling to short-wavelength phonons due to confinement is weak so that broadening of absorption lines is more pronounced than that in bulk materials. Bawendi and co-workers⁹ also investigated the size dependence of the Huang–Rhys factor in CdSe QDs. In their model, the essential parameters include the Stokes shift, the position of emission and excitation, the line width parameter of a normalized Gaussian at each peak location, and the Huang–Rhys factor.

Rudin, Reinecke, and Segall conducted a study on temperature dependence of exciton line widths in semiconductors using a Green's function approach.¹⁰ Treating exciton–phonon coupling perturbatively, they take into account the effects of resonant coupling between photons and excitons to form polaritons. Results for LO-phonon coupling are found to be in good agreement with measurements, although for acoustic-phonon coupling their results are lower than experimental estimates.

Knox et al.¹¹ investigated the temperature dependence of the zero-phonon lines (ZPLs) of chromophores in host media based on a multimode Brownian oscillator (BO) model. Their results show that in the low temperature limit the line widths of the ZPLs vanish since the fluctuations of the bath are suppressed. Besides, the line shapes of the ZPLs are found to take on an asymmetric form due to the fact that the zero-temperature bath can only accept rather than provide energy quanta to the system.

* Corresponding author. E-mail: YZhao@ntu.edu.sg.

The variation of the line widths is found to be strongly dependent on the precise form of the spectral density according to their analysis of the systems in sub-Ohmic dissipative baths. Dependence of the spectra line shapes on different parameters have also been carried out in their paper. Results show that the widths and the intensities of the phonon sidebands are determined by the temperature, the Huang–Rhys factor, and the coefficient of bath damping. However, only low temperature cases with a Huang–Rhys factor of 1.8 were investigated in their work.

Jang, Cao, and Silbey¹² examined the temperature dependence of the ZPLs and the overall absorption line shape based on a model which describes a two-level chromophore linearly coupled to a bath of harmonic oscillators on the basis of an accurate approximation of a hyperbolic cotangent function [the dissipative two-level system (TLS)]. Their expressions of the line shape functions are applicable to arbitrary temperature and can be extended to a general spectral density. The widths of the ZPLs in the strong-coupling limit depend linearly on temperature. In the weak-coupling limit, features such as asymmetric line shape appear for low temperatures. The effects of decay lifetimes, nonlinear system–bath couplings, and anharmonic bath modes on the line shape broadening are not considered in their model.

In this paper, we use the BO model as a starting point to map out the control-parameter space of the line widths for the ZPLs and the phonon sidebands with the phonon occupation number equal up to 2. Detailed discussions and comparisons between our results and what has been previously obtained by other authors are provided. The paper is organized as follows: In section II the Brownian oscillator model is introduced, and its connection to the Huang–Rhys theory is discussed. In section III we calculate the line widths of the ZPLs and the phonon sidebands using the BO model, and results are compared with those from other studies. Conclusions are given in section IV.

II. The Brownian Oscillator Model

To treat the phonon broadening effect and examine various factors that influence the widths of phonon sidebands, we employ a simplified form of the BO model.^{13–17} The BO model introduces dissipation effects that are omnipresent in solids into a harmonic oscillator system by coupling the system oscillators linearly to bath modes with a continuous spectrum. In such a model system, there is a two-electronic-level system with some primary nuclear coordinates coupled linearly to it and to the harmonic bath. The primary phonons can be those of the host medium or pseudolocalized modes associated with the guest atoms or molecules. The Hamiltonian of the system^{13,14} is given by

$$H = |g\rangle H_g \langle g| + |e\rangle H_e \langle e| + H' \quad (1)$$

where

$$H_g = \sum_j \left[\frac{p_j^2}{2m_j} + \frac{1}{2} m_j \omega_j^2 q_j^2 \right] \quad (2)$$

$$H_e = \hbar \omega_{eg}^0 + \sum_j \left[\frac{p_j^2}{2m_j} + \frac{1}{2} m_j \omega_j^2 (q_j + d_j)^2 \right] \quad (3)$$

and

$$H' = \sum_n \left[\frac{P_n^2}{2m_n} + \frac{1}{2} m_n \omega_n^2 \left(Q_n - \sum_j \frac{c_{nj} q_j}{m_n \omega_n} \right)^2 \right] \quad (4)$$

Here p_j (P_n), q_j (Q_n), m_j (m_n), and ω_j (ω_n) are the momentum, the coordinate, the mass, and the angular frequency of the j th (n th) nuclear mode of the primary (bath) oscillators, respectively. d_j represents the displacement for the j th nuclear mode in the excited electronic state. $\hbar \omega_{eg}^0$ is the energy separation of the purely electronic levels. H' describes the bath modes and their coupling to the primary oscillators with a coupling strength c_{nj} . The cross terms in $q_j Q_n$ are responsible for damping.¹¹ An energy gap coordinate operator U is defined as

$$U = H_e - H_g - \hbar \omega_{eg}^0 \quad (5)$$

The linear absorption spectrum and the relaxed photoluminescence spectrum can be computed by truncating the cumulant expansion of the spectral response function at second order. To derive the expression of the absorption or photoluminescence line shape, we first get a correlation function for the j th mode from the parameters of the Hamiltonian as

$$C_j(t) = -\frac{1}{2\hbar^2} [\langle U(t) U(0) \rho_g \rangle - \langle U(0) U(t) \rho_g \rangle] \quad (6)$$

where $U(t)$ is the operator U in the interaction representation and ρ_g is the equilibrium ground-state vibrational density matrix:

$$\rho_g = \frac{|g\rangle \langle g| \exp(-\beta \hat{H}_g)}{\text{Tr}[\exp(-\beta \hat{H}_g)]} \quad (7)$$

with $\beta = 1/k_B T$. The Fourier transform of the correlation function $C_j(t)$ has an imaginary part known as the spectral density:

$$\tilde{C}_j''(\omega) = \frac{2\lambda_j \omega_j^2 \omega \gamma_j(\omega)}{\omega^2 \gamma_j^2(\omega) + [\omega_j^2 + \omega \Sigma_j(\omega) - \omega^2]^2} \quad (8)$$

Here $2\lambda_j$ is the j th-mode contribution to the Stokes shift

$$2\lambda_j = \frac{m_j \omega_j^2 d_j^2}{\hbar} \quad (9)$$

One can alternatively write $\lambda_j = S_j \hbar \omega_j$, where S_j is the well-known dimensionless Huang–Rhys factor characterizing the strength of electron–LO-phonon interactions.¹⁸ $\gamma_j(\omega)$ is the spectral distribution function describing the coupling between the primary oscillator and the secondary bath oscillators:

$$\gamma_j(\omega) = \frac{\pi}{m_j} \sum_n \frac{c_{nj}^2}{2m_n \omega_n^2} [\delta(\omega - \omega_n) + \delta(\omega + \omega_n)] \quad (10)$$

$\Sigma_j(\omega)$ is the real part of the self-energy related to the spectral distribution function by the Kramers–Kronig relations¹⁹

$$\Sigma_j(\omega) = -\frac{1}{\pi} \mathcal{P} \int_{-\infty}^{\infty} d\omega' \frac{\gamma_j(\omega')}{\omega' - \omega} \quad (11)$$

where \mathcal{P} stands for the Cauchy principal part of the integral.

In the present study, we adopt a simple form of the BO model in which only a single primary oscillator with frequency ω_l (for example, the LO phonons) is considered and its coupling strength with the bath modes is assumed to be a constant (i.e., $\gamma_j(\omega) = \text{constant}$, called the Markovian or Ohmic limit) to compute PL spectra. Our study of non-Markovian baths with a Drude damping kernel reveals that even for a cutoff frequency that is only comparable to the primary phonon frequency, the non-Markovian spectra are similar in shape to the Markovian ones. This is specially true for the underdamped case, which was the case under investigation here. For this simple constant damping case, the spectral density function reads¹⁴

$$\tilde{C}''(\omega) = \frac{2\lambda_l \omega_l^2 \omega \gamma_l}{\omega^2 \gamma_l^2 + (\omega_l^2 - \omega^2)^2} \quad (12)$$

where the real part of the self-energy, $\Sigma_r(\omega)$, is set to zero.

The spectral response function $g(t)$ can be expressed in terms of the frequency-domain correlation function $C''(\omega)$

$$g(t) = -\frac{1}{2\pi} \int_{-\infty}^{\infty} d\omega \frac{C''(\omega)}{\omega^2} [1 + \cot(\beta\hbar\omega/2)] (e^{-i\omega t} + i\omega t - 1) \quad (13)$$

The absorption line shape can be then obtained from the spectral response function $g(t)$:

$$\sigma_{\text{abs}}(\omega) = \frac{1}{\pi} \text{Re} \int_0^{\infty} \exp[i(\omega - \omega_{\text{eg}}^0 - \lambda)t - g(t)] dt \quad (14)$$

III. Width of Phonon Sidebands

The control parameters used for the width study are S , T , and γ (listed in Table 1). The dimensionless Huang–Rhys factor S , an indicator of the coupling strength between the electronic and nuclear degrees of freedom, ranges from $S = 0.5$ (weak coupling) to $S = 2.25$ (strong coupling). The temperature ranges from 25 to 100 K (or from 1.7 to 8.6 meV). The BO model with an Ohmic bath in our study is underdamped, i.e., γ (30–120 cm^{-1}) is much less than the primary phonon frequency $\omega_{\text{LO}} = 600 \text{ cm}^{-1}$ (73.7 meV). Only for low temperatures ($T \ll \omega_{\text{LO}}$) and weak bath dissipation ($\gamma \ll \omega_{\text{LO}}$) are the phonon sidebands well-resolved, so that their line widths can be studied.

Three series of representative absorption spectra demonstrating dependence of the line shapes on the control parameters S , T , and γ are shown in Figures 1, 2 and 3, respectively. Since this work focuses primarily on the line widths, the full width at half-maximum (fwhm) is used to illustrate the effects of S , T , and γ on the spectra obtained by the BO model (cf. insets of Figures 1–3). The line shape as well the line width shows interesting dependence on the control parameters; detailed discussions for each control parameter will be carried out in later sections. The effects of each control parameter on the ZPL line shape are also compared in Figure 4. The control parameters have different effects on the ZPL line shape. From Figure 4a, S has a very significant effect on the line shape change of the

TABLE 1: Data Set of the Three Control Parameters for Line Width Studies^a

T (K)	25	50	75	100				
γ (cm^{-1})	30	60	90	120	150	180		
S	0.5	0.75	1.0	1.25	1.5	1.75	2.0	2.25

^a The primary oscillator frequency $\omega_{\text{LO}} = 600 \text{ cm}^{-1}$ in all cases.

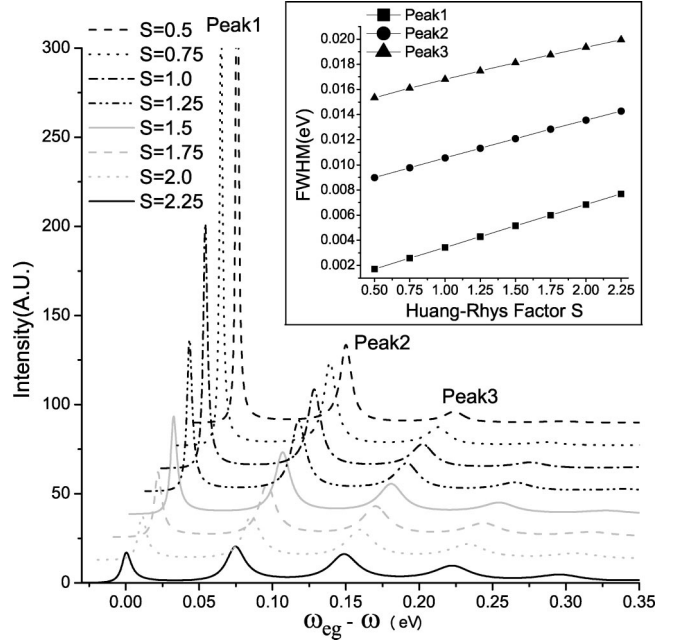


Figure 1. Effect of S on BO spectra. The damping factor and temperature for the spectra are held fixed, where $\gamma = 60 \text{ cm}^{-1}$ and $T = 100 \text{ K}$. The inset is the fwhm vs S plot for various peaks.

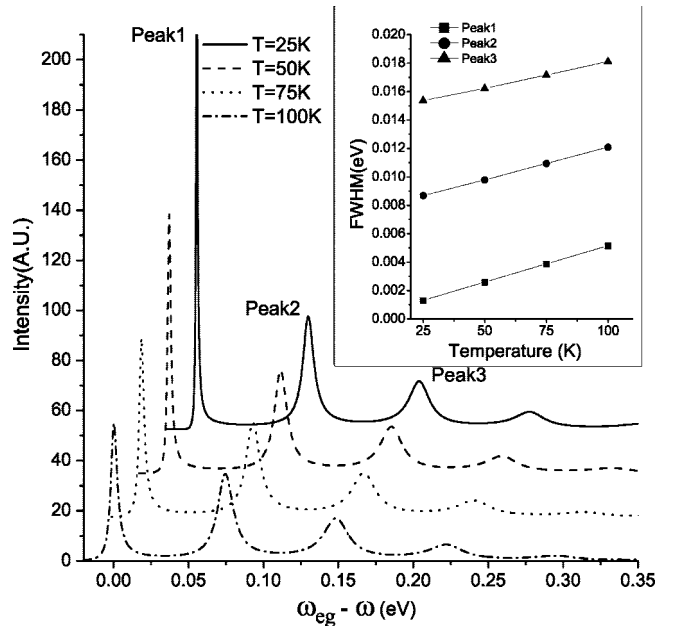


Figure 2. Effect of T on BO spectra. The damping factor and the Huang–Rhys factor for the spectra are kept fixed, where $\gamma = 60 \text{ cm}^{-1}$ and $S = 1.5$. The inset is the fwhm vs T plot for various peaks.

ZPL as it increases from 0.5 (weak coupling) to 2.0 (strong coupling), as shown in Figure 4b,c. T and γ can reduce the intensities of the ZPLs; however, the overall effects of T and γ on the line shape of ZPL are not as great compared to those of S .

A. Effect of Huang–Rhys Factor. As shown in Figure 1, the Huang–Rhys factor S has a dominant effect on the overall

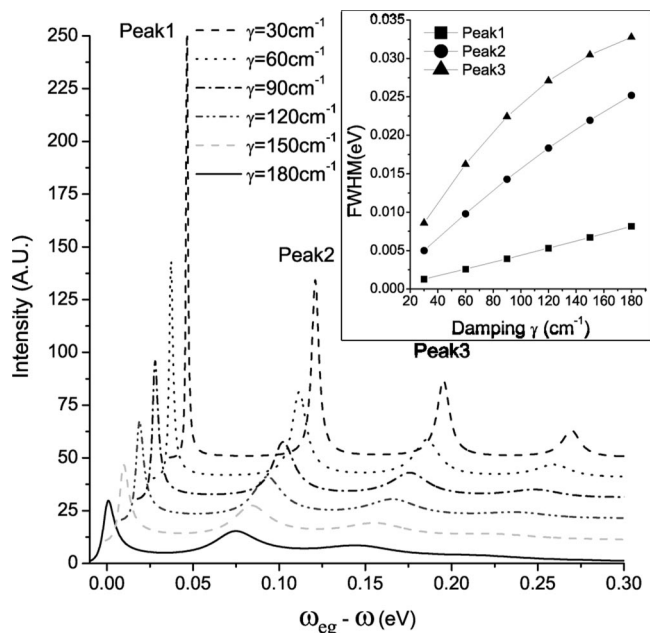


Figure 3. Effect of γ on BO spectra. The temperature and the Huang–Rhys factor S are 50 K and 1.5, respectively, for each γ value. The inset is the fwhm vs γ plot for various peaks.

line shape. Without the coupling to the bath phonons, the Huang–Rhys theory¹⁸ gives a Poisson distribution for phonon side peaks in the absorption spectrum at zero temperature:

$$\sigma_{\text{abs}}(\omega) = \exp(-S_j) \sum_{n=0}^{\infty} \frac{S_j^n}{n!} \delta(\omega - \omega_{eg} - n\omega_j) \quad (15)$$

S here is the intensity ratio between the first and zero phonon lines, and can also be identified with the average number of phonons emitted. For larger S , the Poisson distribution morphs into a Gaussian centered at S . Upon broadening due to bath dissipation and thermal effects, the well-resolved phonon peaks will acquire widths that increase with phonon occupation number n . The width of the individual phonon peak also increases with the temperature, linearly if the bath is Markovian.¹¹ For small S , the ZPL in the absorption spectra tends to a delta function centered at $\omega = \omega_{eg}$. If S increases, the highest peak among the entire spectral line shape will shift from the ZPL to the one representing the largest number of phonons; this phenomenon is consistent with the Huang–Rhys theory.¹⁸

The line width is also found to increase linearly with the Huang–Rhys factor S (cf. inset of Figure 1). Due to the Heisenberg principle, the natural line width is inversely proportional to the excited-state lifetime of the chromophore without interacting with the environment. The line width will increase if the chromophore is interacting with a host medium such as the Markovian bath in the BO model. The interaction of the chromophore with the dissipative bath described by T and γ can reduce the excited-state lifetime. This will lead to the broadening of the ZPLs and phonon sidebands. For a given set of γ and T , the excited-state lifetime decreases further as S increases. This results in further broadening of the ZPLs and phonon sidebands.

Results from fitting the line width data of the ZPLs ($n = 0$) and the phonon sidebands ($n = 1$ and 2) using straight lines are shown in Table 2. The slopes of the fitting lines tend to decrease slightly with increasing n . Due to the

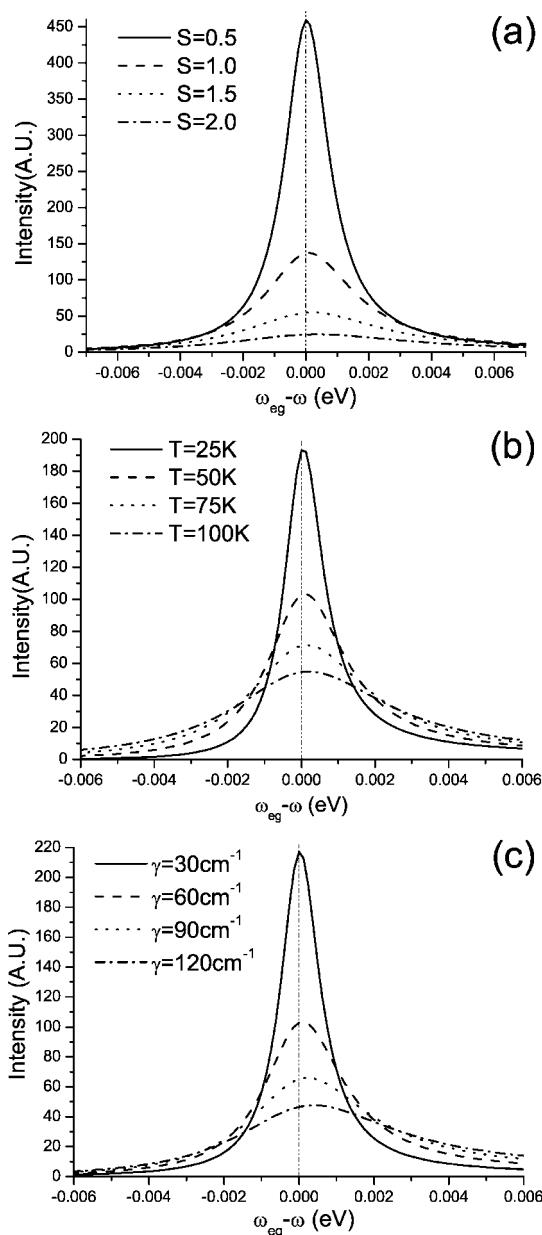


Figure 4. Line shape of the ZPLs from (a) Figure 1, (b) Figure 2, and (c) Figure 3. The control parameters are as follows: (a) $S = 0.5$ –2.0 (interval = 0.5), $\gamma = 60 \text{ cm}^{-1}$, $T = 100 \text{ K}$. The ZPLs with $S = 0.75$, 1.25, 1.75, and 2.25 are omitted for clarity. (b) $T = 25$ –100 K (interval = 25 K), $\gamma = 60 \text{ cm}^{-1}$ and $S = 1.5$. (c) $\gamma = 30$ –120 cm^{-1} (interval = 30 cm^{-1}), $T = 50 \text{ K}$ and $S = 1.5$. The ZPLs with $\gamma = 150$ and 180 cm^{-1} are omitted for clarity.

TABLE 2: Linear Fitting Results for the Inset of Figure 1^a

peaks	intercept (eV)	error	slope (eV)	error
1	1.44×10^{-5}	5.98×10^{-6}	0.003 42	4.01×10^{-6}
2	0.007 51	3.16×10^{-5}	0.003 03	2.12×10^{-5}
3	0.014 13	5.0×10^{-5}	0.002 62	4.03×10^{-5}

^a The control parameters for Figure 1 are $S = 0.5$ –2.25 (interval = 0.25), $\gamma = 60 \text{ cm}^{-1}$, and $T = 100 \text{ K}$.

exponential factor in eq 15, the intensities of the peaks tend to decline with increasing S . For larger S , an increase in number of visible peaks is observed. Such an effect can be understood as a result of the shift of the center-of-mass of the overall line shape to higher energy due to stronger electron–phonon coupling. Another important phenomenon to be noted is that the line shape of the ZPLs tends to become

TABLE 3: Linear Fitting Results for the Inset of Figure 2^a

peaks	intercept (eV)	error	slope (eV/K)	error
1	2.92×10^{-5}	3.56×10^{-8}	5.12×10^{-5}	5.2×10^{-8}
2	0.007 54	1.86×10^{-5}	4.53×10^{-5}	2.72×10^{-7}
3	0.014 42	4.61×10^{-5}	3.68×10^{-5}	6.73×10^{-7}

^a The control parameters are $T = 25$ – 100 K (interval = 25 K), $S = 1.5$, and $\gamma = 60$ cm⁻¹.

more asymmetric with increasing S (cf. Figure 4a). However, The dimensionless S cannot solely determine the line width of the ZPLs and the phonon sidebands. The effects of T and γ must be taken into account.

B. Effects of Temperature. As demonstrated in Figure 2, temperature has a less significant effect on both the line shape and the line width when compared to S . For the case of $S = 1.5$ and $\gamma = 60$ cm⁻¹, there are five visible peaks in the spectra regardless of the temperature. Although increasing T from 25 to 100 K tends to broaden the peaks and reduce their intensities, the number of the visible phonon sideband peaks does not change. The thermal effect is more related to the excitation of the dissipative bath modes; thus the temperature only has a moderate effect to the spectra unless the temperature is high ($k_B T \gg \hbar\omega_{LO}$) enough. Therefore, at higher temperatures, more bath modes will be excited; the dissipation rate will be increased accordingly, resulting in a broadening effect on the ZPLs and phonon sidebands. It is also worthwhile to note that the ZPL line shape at lower temperature (25 K) shows asymmetry, a feature that becomes less obvious with increasing temperature (cf. Figure 4b).

Knox et al.¹¹ showed that the line width of the $n = 0$ (ZPL) and $n = 1$ peaks can change linearly with the temperature for the Ohmic baths, and the ZPL line width approaches zero in the low temperature limit. This linear dependence is confirmed here. In addition to the first two peaks with $n = 0$ and 1, we find that the linear dependence of the line width on T can be extended to the third peak (cf. Figure 2) with $n = 2$. This feature should not be an exception, since under the Ohmic damping, the system composed of two electronic degrees of freedom and one primary oscillator is linearly coupled to the bath. Thus, for all thermal occupation numbers of the primary oscillator, the linear dependence of the line width on temperature should be valid.¹¹ In addition, the feature of the linear dependence of the line width on temperature for peaks 2 and 3 is in good agreement with results of Xu et al.²⁰ for GaN. However, one notable feature in the BO model is that the line width of the phonon sidebands for $n = 2$ is greater than that for $n = 1$, which differs from what was obtained by Xu et al.

The line width depends monotonically on n when all control parameters are fixed. In the other words, the broadening effect due to the presence of the bath will be enhanced with increasing n . Table 3 shows the slope change of the line width as a function of temperature for $n = 0$ (ZPLs), 1, and 2. It is observed that, as n increases, the slope decreases.

C. Effect of Bath Damping. The damping factor γ is found to have strong influences on the line shapes and the line widths of the calculated spectra. As shown in Figure 3, increasing γ can reduce the intensities of the peaks while broadening the line widths of the spectra. However, it is important to note that only for the ZPLs are the line widths linearly dependent on γ . With increasing n , the line width dependence on γ takes on a quadratic component. Then the data points of the line widths as a function of γ in the inset of Figure 3 can be fitted using a polynomial of γ up to second order (cf. Table 4). If n increases, the feature in the inset of Figure 3 becomes obvious; this is due to a large increase of $|b|$ (the coefficient of the γ^2 term) relative to $|a|$ (the coefficient of the γ term). However, γ has

TABLE 4: Fitting Results for the Inset of Figure 3^a

peaks	d_0	error	a	error	b	error
1	3×10^{-5}	5×10^{-6}	0.34	9×10^{-4}	1.34	0.04
2	-3×10^{-4}	4×10^{-5}	1.48	0.006	-14.79	0.24
3	-2.4×10^{-4}	2×10^{-4}	2.59	0.04	-49.9	1.5

^a The fitting function is $y = d_0 + ax + bx^2$. The y -axis is the line width and the x -axis is γ . The unit for γ is converted from cm⁻¹ to eV. The units for the fitting parameters d_0 , a , and b are eV, eV·cm, and eV·cm², respectively. The control parameters for Figure 3 are $\gamma = 30$ – 180 cm⁻¹ (interval = 30 cm⁻¹), $S = 1.5$, and $T = 50$ K.

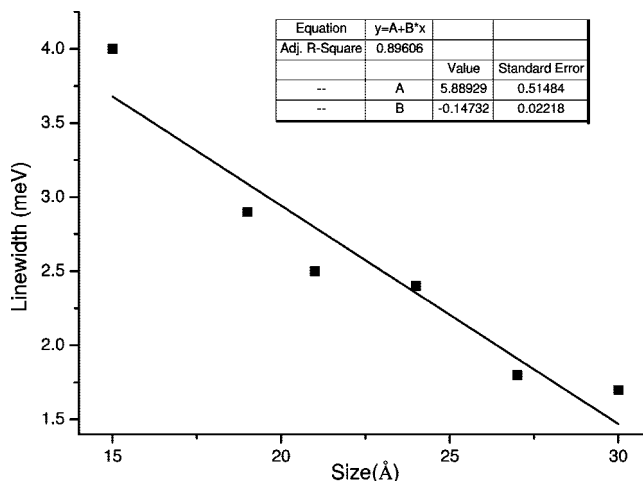


Figure 5. ZPL line width dependence on CdSe quantum-dot size fitted with a straight line, where the information for the ZPL line width is obtained from the band-edge absorption spectra. The line width data are taken from Table 1 of ref 9.

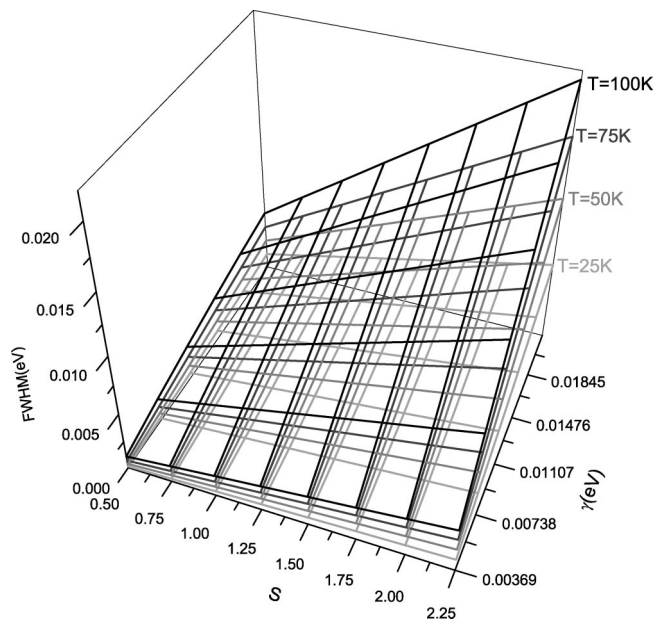


Figure 6. Line width dependence on S , T , and γ for peak 1 (ZPL, $n = 0$) represented by a series of isothermal surfaces. The magnitude of the temperature is shown by the gray scale of the fonts and the lines; the darker the fonts and the lines, the higher the temperature.

almost no effect on the asymmetry of the ZPL line shape (cf. Figure 4c). This asymmetric feature of the ZPL line shape can be eliminated only at very high temperature ($k_B T \gg \hbar\omega_{LO}$) for $\gamma \gg \omega_{LO}$.¹³

Norris et al.⁹ investigated the size dependence of the exciton fine structures in the CdSe quantum dots by fitting the emission and absorption curves with a large number of parameters

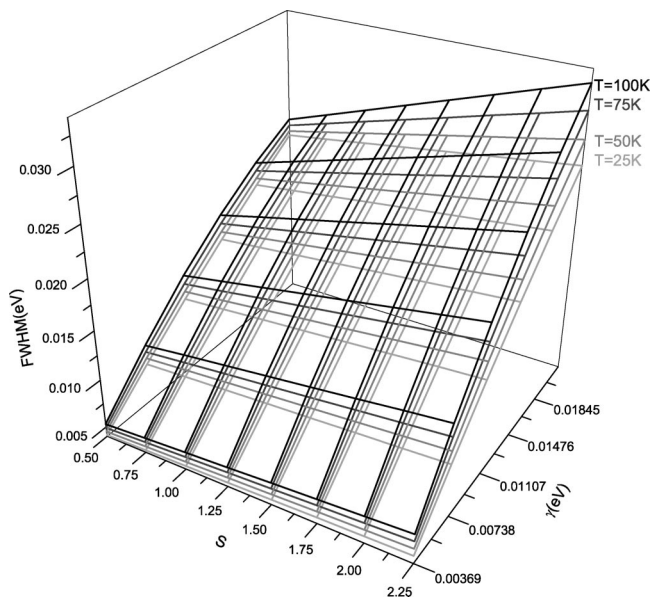


Figure 7. Line width dependence on S , T , and γ for peak 2 ($n = 1$) represented by a series of isothermal surfaces. The magnitude of the temperature is shown by the gray scale of the fonts and the lines; the dark the fonts and the lines, the higher the temperature.

including a width parameter for the ZPL and each phonon sideband. Their results show that the line width decreases with increasing quantum-dot size. This feature is prominent for the ZPLs when S is close to 0.5 or weaker. Figure 5 shows widths of the ZPLs from ref 9 as a function of quantum-dot size fitted with a straight line. Note that S are lower than 0.5 for the chosen data. As shown in Figure 5, the line width linearly decreases with increasing dot size. Cerrullo et al.²¹ found that the damping is proportional to $1/R$ (where R is the radius of the quantum dots), which indicates that smaller quantum dots will have a higher damping. In our model, the line widths of the ZPLs depend linearly on γ for weak-coupling cases (e.g., $S = 0.5$), which is in agreement with those of Cerrullo et al.²¹ and Norris et al.⁹

Jang, Cao, and Silbey¹² defined a real positive number m that was related to different spatial dimensions in the deformation potential model,²² and reported a reduction in temperature dependence of the line width with increasing m . For the weak-coupling limit, the spectral features show critical dependence on m . Specifically, the dependence of the ZPL line width on temperature vanishes when $m = 3$ since the ZPL line shape function has the form of a delta function for the weak-coupling ($S \ll 1$) limit. In their work, the ZPL line width W_m (D_n is used in ref 12), a function of m , is related to the temperature via a polynomial of θ ($1/\theta = k_B T/\hbar\omega_c$) in the strong-coupling limit ($S \gg 1$)

$$W_m^2(\theta) = 1 + \frac{2}{(1 + \theta)^{m+1}} + \frac{2}{(1 + 2\theta)^{m+1}} + \frac{2}{m\theta(1 + 5\theta/2)^m} \quad (16)$$

The widths show monotonic crossover from the zero temperature limit to the high temperature asymptotic behavior, $[2k_B T/(n\hbar)]^{1/2}$. The width is linearly dependent on temperature at the crossover region, while the approach to the high temperature limit is faster for smaller m . For $S > 1$ the linear dependence of the line width on temperature in our model is in agreement with Jang et al. if m in their model is set to 1.

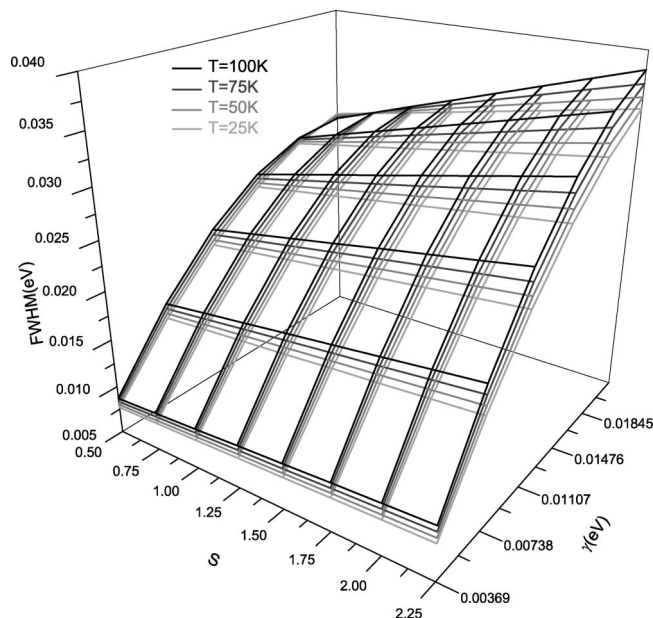


Figure 8. Line width dependence on S , T , and γ for peak 3 ($n = 2$) represented by a series of isothermal surfaces. The magnitude of the temperature is shown by the gray scale of the fonts and the lines; the dark the fonts and the lines, the higher the temperature.

According to Jang et al., the spectral density can be written as

$$J_m(\omega) = \frac{\alpha_m}{m!} \frac{\omega^m}{\omega_c^{m-1}} e^{-\omega/\omega_c} \quad (17)$$

where α_m is a dimensionless constant determining the strength of the coupling, and ω_c is the cutoff frequency dictating the spectral width of the bath. If $m = 1$, eq 17 is reduced to

$$J(\omega) = \alpha\omega e^{-\omega/\omega_c} \quad (18)$$

According to Leggett et al.,²³ this expression of the spectral density is the Ohmic dissipative bath, and for $m > 1$ (< 1), eq 17 represents a super-Ohmic (sub-Ohmic) bath. Thus the agreement between our result ($S > 1$) and that of Jang et al. ($m = 1$) is expected since both cases are Ohmic baths. For both the dissipative TLS model and the BO model, the spectral density is defined as

$$J(\omega) \equiv \frac{\pi}{2} \sum_n \frac{c_n^2}{M_n \omega_n} \delta(\omega - \omega_n) \quad (19)$$

where M_n and ω_n describe the mass and the frequency of the n th bath oscillator, respectively, and c_n is the coupling strength between the n th bath phonon mode and the primary oscillator. In the continuum limit, the Fourier transform of the retarded memory-friction kernel is²⁴

$$\tilde{\gamma}(\omega) = \lim_{\epsilon \rightarrow 0^+} \frac{-i\omega}{M} \frac{2}{\pi} \int_0^\infty d\omega' \frac{J(\omega')}{\omega' \omega'^2 - \omega^2 - i\epsilon \operatorname{sgn}(\omega)} \quad (20)$$

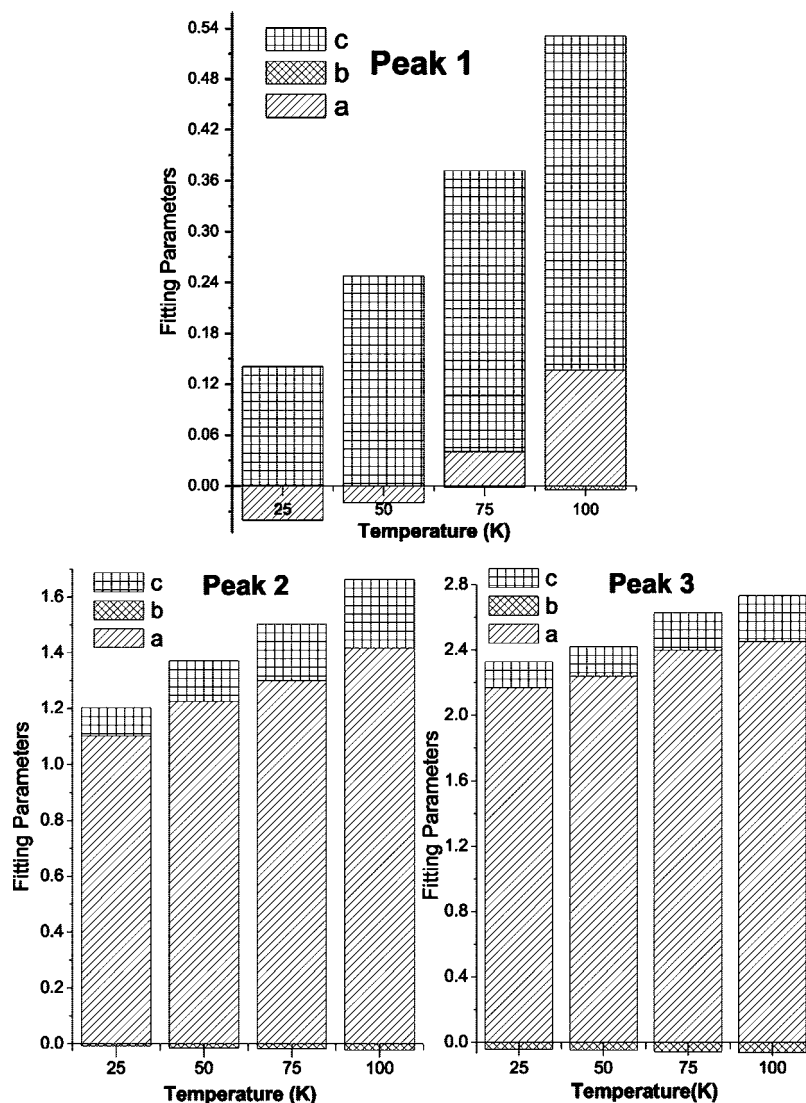


Figure 9. Fitting parameters for eq 23 shown as cumulative bars for peaks 1 ($n = 0$), 2 ($n = 1$), and 3 ($n = 2$). The width of the bars is 20 in the figures for clarity, and the x-axes are all temperatures. The fitting parameter b is divided by 1000 due to the small value of γ^2 .

where ϵ is an infinitesimal real number. In this limit, the function $\tilde{\gamma}(\omega)$ requires a smooth real part

$$\tilde{\gamma}'(\omega) = J(\omega)/M\omega \quad (21)$$

where M is the mass of the primary oscillator. In the Ohmic limit the damping of the bath does not depend on the frequency (i.e., $\tilde{\gamma}'(\omega) = \gamma$); the spectral density then has the following form:

$$J(\omega) = M\gamma\omega \quad (22)$$

Thus the two different spectral densities described by eq 18 and eq 22 are identical for $\omega \ll \omega_c$ in eq 18. In general, one needs to carry out a transformation between the BO model and the dissipative TLS model.

D. Combined Effect of Control Parameters. The discussions above provide a picture on how the line width of the phonon sidebands depends on the control parameters: S , T , and γ . As shown in Figures 1–3, the widths are found to increase with increasing n . The dependence of the widths on S , T , and

γ also changes with n . For larger n , the influence on line widths from S or T becomes less significant compared to γ .

In order to map out the parameter space for the BO line widths, a thorough study has been carried out for the dependence of the line width of the ZPLs ($n = 0$) and phonon sidebands ($n = 1, 2$) on S and γ at fixed T . The line width information is taken from the absorption spectra calculated by eq 14. Results are displayed in Figures 6, 7, and 8 for $n = 0, 1$, and 2, respectively. From Figures 6–8, it is found that the line widths of $n = 0, 1$, and 2 peaks depend strongly on γ and S for a given temperature T . The isothermal plots of the ZPL ($n = 0$) line widths as a function of S and γ are shown in Figure 6. As T increases, the isothermal surfaces of the line widths tend to rise accordingly. For $n = 0$, the temperature is identified as the dominant parameter in determining the line widths. It is also very interesting to note that, in Figure 6, the weak-coupling line widths (e.g., $S = 0.5$) have a weaker temperature dependence compared to the strong-coupling ones (e.g., $S = 2.25$). Figures 7 and 8 display similar isothermal surfaces for $n = 1$ and $n = 2$ peaks, respectively. The major difference between Figures 6 and 7 is the decrease of the intersurface distances in Figure 7. Therefore, the effect of T on the line width of the $n = 1$ peak becomes less dominant compared to the ZPL. In

Figure 8 ($n = 2$), the intersurface distance drops further, and the quadratic dependence of the isothermal surfaces on γ becomes apparent. Thus, the ZPLs are much more sensitive to the change of the control parameters compared to the phonon sidebands. As n increases, the isothermal surfaces show less changes with varying control parameters. From this together with the results obtained previously from the line shape analysis, a detailed description of how phonon-sideband line widths vary with the control parameters S , T , and γ now emerges. Now we denote the line width of the n th ($n = 0, 1, 2, \dots$) peak for temperature T by $D_n(T)$ (eV). For example, $D_0(T)$ is the line width of the ZPL, $D_1(T)$ is the line width of the first phonon sideband, and $D_2(T)$ is the line width of the second phonon sideband. In order to obtain the dependence of the line width $D_n(T)$ on the control parameters, we adopt a simple fitting function consisting of γ and S to fit the isothermal surfaces in Figures 6–8. The fitting function can be described by a simple polynomial up to second order as

$$D_n(T) = a\gamma + b\gamma^2 + c\gamma S \quad (23)$$

where a (eV·cm), b (eV·cm²), and c (eV·cm) are the fitting parameters. Results are shown in Figure 9. In our study, the numerical value for the largest γ^2 is less than 1×10^3 ; hence we divide b by 1000 in Figure 9. The relative importance of the fitting parameters a , b , and c is shown in Figure 9 as the relative heights of the cumulative bars. As shown in Figure 9, the dominant parameter for peak 1 or the ZPL is c . Hence, the major contribution to $D_0(T)$ is from the $c\gamma S$ term. This is in agreement with the work of Knox et al.¹¹

As n increases from $n = 0$ to 2 (cf. Figures 6–8), the shape of the isothermal surfaces changes considerably. This is due to the fact that the line widths of the satellite peaks ($n \geq 1$) show varying S , T , and γ dependence compared to the ZPLs. For $n = 1$ and 2, γ has a more significant effect on broadening than S or T . As discussed in the previous sections, the dependence of the width on γ changes from linear to quadratic as n increases (cf. Table 4); this quadratic dependence tends to be more apparent if n increases. The relative importance of the control parameters changes with n as shown in the lower panels of Figure 9 for peaks 2 and 3. The major difference is the rising of the significance of the fitting parameter a for the $a\gamma$ term in eq 23. Although the fitting parameter c is small for peaks 2 and 3 compared to peak 1, the term $c\gamma S$ is still not negligible. In a similar manner, although the $b\gamma^2$ term in $D_1(T)$ or $D_2(T)$ is small compared to the $a\gamma$ and $c\gamma S$ terms, its contribution is necessary in order to explain the quadratic nature in Figures 7 and 8. The changes in the curvature of the isothermal surfaces with increasing n in Figures 6–8 can be explained by the increasing contribution from the $b\gamma^2$ term and the decreasing contribution from the $c\gamma S$ term in the $D_n(T)$ ($n = 0, 1, 2$) expressions.

IV. Conclusion

The BO model has been employed to treat the fine structures of the phonon broadening effect in a coupled electron–phonon system attached to a dissipative bath. The line shape and the line widths of the spectra are related to the control parameters S , T , and γ of the BO model. In general, the line width of a phonon sideband tends to increase with these control parameters. S determines the general line shape of the spectra, and for given γ and T the line width dependence on S is linear. Specifically, changing S cannot eliminate the asymmetry of the ZPLs at low

temperatures. The temperature T has a considerable effect on the line widths of the ZPLs and the phonon sidebands. At high temperatures, the asymmetry of the ZPLs tends to vanish. The line widths are found to depend strongly on the damping factor γ of a Markovian bath. In summary, a comprehensive study of the line width dependence on temperature, bath dissipation, and electron–phonon coupling has been carried out in this paper, from which we can conclude the following: (1) The construction of a control-parameter space allows for identifying important broadening mechanisms of the ZPLs and the phonon sidebands in a systematic fashion. (2) Line broadening in the BO model can be mainly attributed to the thermal effect and the dissipation of the bath characterized by γ . (3) The Huang–Rhys factor S has an important role in determining the overall line shape; the line widths show a linear dependence on S or T if other parameters are fixed. (4) As n increases from 0 to 2, the line width dependence on γ shows a transition from linear to quadratic.

In addition, our results on the line width dependence agree with those of Norris et al.⁹ and Xu et al.,²⁰ demonstrating the versatility of the BO model in interpreting spectral measurements and extracting from them useful physical quantities such as ω_{LO} , γ , and S . In this work we focus mainly on the underdamped BO model with an Ohmic dissipative bath at low temperatures, and the Huang–Rhys factors used are not large. Further line width studies on underdamped BO models with various non-Ohmic baths and multiple primary phonon modes are now in progress.

Acknowledgment. Support from the Singapore Ministry of Education through the Academic Research Fund (Tier 2) under Project No. T207B1214 is gratefully acknowledged.

References and Notes

- (1) Efros, A. L. *Phys. Rev. B* **1992**, *46*, 7448.
- (2) Nimal, M.; et al. *Phys. Rev. Lett.* **1995**, *75*, 3728.
- (3) Takagahara, T. *J. Lumin.* **1996**, *70*, 129.
- (4) Vasilevskiy, M. I.; et al. *Phys. Rev. B* **2004**, *70*, 035318.
- (5) Staiuber, T.; Zimmermann, R. *Phys. Rev. B* **2006**, *73*, 115303.
- (6) Gurioli, M.; et al. *Phys. Rev. B* **2006**, *73*, 835302.
- (7) Menendez-Proupin, E.; et al. *J. Phys.: Condens. Matter* **2006**, *18*, 7283.
- (8) Schmitt-Rink, S.; Miller, D. A. B.; Chemla, D. S. *Phys. Rev. B* **1987**, *35*, 8113.
- (9) Norris, D. J.; Efros, A. L.; Rosen, M.; Bawendi, M. G. *Phys. Rev. B* **1996**, *53*, 16347.
- (10) Rudin, S.; Reineck, T. L.; Segall, B. *Phys. Rev. B* **1990**, *42*, 11218.
- (11) Knox, R. S.; Small, G. J.; Mukamel, S. *Chem. Phys.* **2002**, *281*, 1.
- (12) Jang, S.; Cao, J.; Silbey, R. J. *J. Phys. Chem. B* **2002**, *106*, 8313.
- (13) Mukamel, S. *Principles of Nonlinear Optical Spectroscopy*; Oxford University Press: Oxford, 1995.
- (14) Zhao, Y.; Knox, R. S. *J. Phys. Chem. A* **2000**, *104*, 7751.
- (15) Shi, S. L.; Li, G. Q.; Xu, S. J.; Zhao, Y.; Chen, G. H. *J. Phys. Chem. B* **2006**, *110*, 10475.
- (16) Xu, S. J.; et al. *Appl. Phys. Lett.* **2006**, *88*, 083123.
- (17) Su, L. T.; Tok, A.; Zhao, Y.; Ng, N.; Boey, F.; Woodhead, J. L.; Summers, C. J. *J. Phys. Chem. B* **2008**, *112*, 10830.
- (18) Huang, K.; Rhys, A. *Proc. R. Soc. (London)*, **A 1950**, *204*, 406.
- (19) Jackson, J. D. *Classical Electrodynamics*, 2nd ed.; John Wiley & Sons: New York, 1975.
- (20) Xu, S. J.; Li, G. Q.; Xiong, S. J.; Che, C. M. *J. Appl. Phys.* **2006**, *99*, 073508.
- (21) Cerrullo, G.; Silvestri, S. De.; Banin, U. *Phys. Rev. B* **1999**, *60*, 1928.
- (22) Kikas, J.; Suisalu, A.; Zazubovich, V.; Vois, P. *J. Chem. Phys.* **1996**, *104*, 4434.
- (23) Leggett, A. J.; Chakravarty, S.; Dorsey, A. T.; Fisher, M. P. A.; Garg, A.; Zwerger, W. *Rev. Mod. Phys.* **1987**, *59*, 1.
- (24) Weiss, U. *Series in Modern Condensed Matter Physics: Quantum Dissipative Systems*, 2nd ed.; World Scientific Publishing: Hackensack, NJ, 1999.